Energy 36 (2011) 4531–4541

Contents lists available at ScienceDirect

Energy

journal homepage: www.elsevier.com/locate/energy

Heat transfer and friction in solar air heater duct with W-shaped rib roughness on absorber plate

Atul Lanjewar*, J.L. Bhagoria, R.M. Sarviya

Department of Mechanical Engineering, Faculty of Engineering, Maulana Azad National Institute of Technology, Bhopal 462051, India

ARTICLE INFO

Article history:
Received 24 September 2010
Received in revised form
17 February 2011
Accepted 19 March 2011
Available online 4 May 2011

Keywords:
Artificial roughness
Heat transfer enhancement
Solar air heater
Thermo-hydraulic performance
W-ribs

ABSTRACT

Artificial roughness in form of ribs is convenient method for enhancement of heat transfer coefficient in solar air heater. This paper presents experimental investigation of heat transfer and friction factor characteristics of rectangular duct roughened with W-shaped ribs on its underside on one broad wall arranged at an inclination with respect to flow direction. Range of parameters for this study has been decided on basis of practical considerations of system and operating conditions. Duct has width to height ratio (W/H) of 8.0, relative roughness pitch (p/e) of 10, relative roughness height (e/D_h) 0.018–0.03375 and angle of attack of flow (α) 30–75°. Air flow rate corresponds to Reynolds number between 2300 –14,000. Heat transfer and friction factor results have been compared with those for smooth duct under similar flow and thermal boundary condition to determine thermo-hydraulic performance. Correlations have been developed for heat transfer coefficient and friction factor for roughened duct.

1. Introduction

Solar air heaters are simple in design and construction. They are widely used as collection devices having applications such as space heating and crop drying. Efficiency of flat plate solar air heater is low because of low convective heat transfer coefficient between absorber plate and flowing air that increases absorber plate temperature, leading to higher heat losses to environment. Low value of heat transfer coefficient is due to presence of laminar sub-layer that can be broken by providing artificial roughness on heat transferring surface [1]. Efforts for enhancing heat transfer have been directed toward artificially destroying or disturbing this laminar sub-layer. Artificial roughness in form of ribs and in various configurations has been used to create turbulence near wall or to break laminar sub-layer. Artificial roughness results in high frictional losses leading to more power requirement for fluid flow. Hence turbulence has to be created in region very close to heat-transferring surface for breaking viscous sub-layer. Core fluid flow should not be unduly disturbed to limit increase in pumping requirement. This is done by keeping height of roughness elements small in comparison to duct dimensions [2]. Application of artificial roughness in solar air heater owes its origin to several investigations carried out for enhancement of cooling of turbine blades' passage. Several investigations have been carried out to study effect of artificial roughness on heat transfer and friction factor for two opposite roughened surfaces by Han [3,4], Han et al. [5–7], Wright et al. [8], Lau et al. [9–11], Taslim et al. [12,13], Liou and Hwang [14], Han and Park [15], Park et al. [16], Han and Zhang [17], Kiml et al. [18] and Gao et al. [19] and correlations were developed by different investigators.

Prasad and Mullick [20], Prasad and Saini [21], Gupta et al. [22], Saini and Saini [23], Karwa et al. [24], Verma and Prasad [25], Bhagoria et al. [26], Momin et al. [27], Karwa [28], Sahu and Bhagoria [29], Jaurker et al. [30], Karmare and Tikekar [31], Layek et al. [32], Aharwal et al. [33], Varun et al. [34], Saini and Verma [35] and Saini and Saini [36] have carried out investigations on rib roughened absorber plate of solar air heater which has only one roughened wall and three smooth walls. Correlations for heat transfer coefficient and friction factor have been developed for such systems. Prasad and Mullick [20] used artificial roughness in form of fine wires in solar air heater duct. Prasad and Saini [21] used transverse small diameter wire as roughness element. Gupta et al. [22] investigated effect of relative roughness height and angle of attack on heat transfer and friction factor for inclined circular wire ribs for relative roughness pitch of 10 and 7.5. Saini and Saini [23] investigated performance of expanded metal mesh geometry by varying relative long way length and relative short way length of mesh. Karwa et al. [24] investigated effect of rib chamfer angle(Φ)

* Corresponding author. Tel.: +91 755 2670496; fax: +91 755 2670562.
E-mail address: lanjewar_atul@yahoo.com (A. Lanjewar).

0360-5442/$ – see front matter © 2011 Elsevier Ltd. All rights reserved.
doi:10.1016/j.energy.2011.03.054

and duct aspect ratio on heat transfer and friction factor using integral chamfered ribs. Chamfer angle of 15° gave highest Stanton number as well as highest friction factor. Verma and Prasad [25] investigated effect of relative roughness height and relative roughness pitch on heat transfer and friction factor for circular ribs. Maximum thermo-hydraulic performance was reported for roughness Reynolds number of 24. Bhagoria et al. [26] investigated wedge shaped transverse integral rib roughness. Maximum heat transfer occurred for relative roughness pitch of 7.57. Wedge angle of 10° gave maximum enhancement of heat transfer. Momin et al. [27] investigated effect of geometrical parameters of V-shaped rib roughness. Maximum thermo-hydraulic performance occurred for 60°. Karwa [28] investigated effect of transverse, inclined, V continuous and V-discrete pattern ribs on heat transfer enhancement. V pattern ribs were tested pointing upstream and downstream to flow. Based on equal pumping criteria V-down arrangement gave best heat transfer performance. Sahu and Bhagoria [29] investigated using 90° broken transverse ribs on absorber plate of solar air heater. Plate with roughness pitch of 20 mm gave highest efficiency of 83.5%. Jaurker et al. [30] investigated effect of rib-grooved artificial roughness on heat transfer and friction characteristics of solar heater. Thermo-hydraulic performance of rib-grooved duct was superior as compared to ribbed duct only. Karmare et al. [31] investigated using metal grit ribs as roughness. Layek et al. [32] investigated performance of solar air heater using integral transverse chamfered rib groove roughness. Aharwal et al. [33] investigated heat transfer enhancement due to gap in inclined continuous rib arrangement for square cross-section rib. They reported maximum enhancement in Nusselt number and friction factor to be 2.59 and 2.87 times to that of smooth duct respectively. Varun et al. [34] studied heat transfer and friction characteristics using combination of inclined as well as transverse ribs. Saini and Verma [35] investigated performance of solar air heater using dimple shape roughness element. Investigation covered range of Reynolds number (Re) from 2000–12,000, relative roughness height from 0.018–0.037 and relative roughness pitch from 8 to 12. They reported that maximum value of Nusselt number corresponded to relative roughness height of 0.037 and relative roughness pitch of 10. Minimum value of friction factor corresponded to relative roughness height of 0.0289 and relative roughness pitch of 10. Saini et al. [36] studied performance of solar air heater using arc shaped wire as artificial roughness.

Although analytical tools are available for investigating heat transfer problems, but due to complex nature of governing equations and difficulty in getting numerical solutions, researchers have focused greater attention on experimental investigation.

From literature survey it has been found that Han et al. [5] investigated effect of rib shape, angle of attack and pitch to rib height ratio (p/e) on friction factor and heat transfer characteristics of rectangular duct with two side roughened walls. They reported that maximum value of heat transfer and friction factor occurs at relative roughness pitch of 10 and for ribs oriented at 45° angle when compared to ribs at 90° angle of attack or when compared to sand-grain roughness. Thereafter focus of rib turbulators shifted to investigation of high performance ribs. Han et al. [7] studied square channel with V, parallel (angled) and crossed ribs. Results reported that 60 deg (or 45 deg) V-shaped rib performed better than 60 deg (or 45 deg) parallel rib and also better than 60 deg (or 45 deg) crossed rib and 90 deg rib. V-shaped rib produced highest heat transfer augmentation while Λ-shaped rib generated greatest pressure drop. Crossed ribs produced lowest heat transfer enhancement and smallest pressure drop penalty. Lau et al. [9] examined turbulent heat transfer and friction characteristics of fully developed flow of air in square channel with aligned arrays of V-shaped ribs. Angle of attack of V-shaped rib arrays were 45°, 60°, 90° (same as 90° full ribs), 120°, and 135°. 60° V-shaped ribs with $p/e = 10$ had highest ribbed wall heat transfer for given air flow rate and highest channel heat transfer per unit pumping power. Taslim et al. [13] investigated heat transfer and friction factor characteristics of channel roughened with angled and V-shaped ribs. V-shaped ribs were tested pointing upstream and downstream to main flow. They reported that enhancement in heat transfer coefficient for air flow in channel roughened with V-shaped ribs is higher than that roughened with angled ribs as well as 90° ribs of the same geometry. Also V-ribs pointing downstream were slightly better in performance.

Studies of Han et al. [5–7], Wright et al. [8], Lau et al. [9–11] and Taslim et al. [12,13] have not covered wide range of roughness and operating parameters that would be required for selection of roughness parameter to be used in conventional solar air heaters. Most of the investigations carried out so far have applied artificial roughness on two opposite walls with all four walls being heated. However in case of solar air heater, roughness elements are applied to heated wall while remaining three walls are insulated. Heated wall consists of absorber plate and is subjected to uniform heat flux (insolation). This makes fluid flow and heat-transfer characteristics distinctly different from those found in case of two roughened walls and four heated wall duct. Literature survey reveals that inclined and V-ribs give significant enhancement in heat transfer as compared to smooth plate. Secondary flow generated in above two cases has been cited as the main reason. In case of V-ribs four secondary vortices are generated. If the number of vortices is increased then theoretically it should increase heat transfer. But effect on friction needs to be investigated experimentally to evaluate its feasibility. Hence the present investigation has been taken up with objective of experimentation on W-shaped ribs as artificial roughness attached to underside of one broad wall of duct, to collect data on heat transfer and fluid flow characteristics. Data is presented in form of Nusselt number and friction factor plots as a function of geometrical parameters of artificial roughness and thermo-hydraulic performance plots to bring out clearly effect of these parameters and enhancement in heat transfer achieved as result of providing artificial roughness.

2. Experimental program and procedure

An experimental set up has been designed and fabricated to study effect of W-shaped ribs on heat transfer and fluid flow characteristics in rectangular duct for range of parameters decided on basis of practical considerations of system and operating conditions. Experimental duct consists of wooden channel that includes five sections, namely smooth entrance section, roughened entrance section, test section, exit section and mixing chamber as outlined by Duffie and Beckman [37]. G.I. sheet of 20 SWG of 1.5×0.2 m^2 size has been used as an absorber plate and lower surface of plate has been provided with artificial roughness in form of W-shaped copper wires. An electric heater of dimensions identical to that of absorber plate has been used to provide uniform heat flux to absorber plate up to maximum of 1500 Wm^{-2}. Power supply to heater has been provided through variable transformer. Transformer enables heat flux applied to absorber plate to be varied as desired. Schematic diagram of experimental set up and view of plate with roughness geometry of 60° W-shaped ribs are shown in Fig. 1 (a) and (b) respectively. W-shaped roughness elements were fixed below the absorber plate and fast drying epoxy has been applied for gluing roughness elements. Values of system and operating parameters of this investigation are listed in Table 1. Relative roughness pitch (p/e) value has been selected as 10, based on optimum value of this parameter reported in literature [5,27].

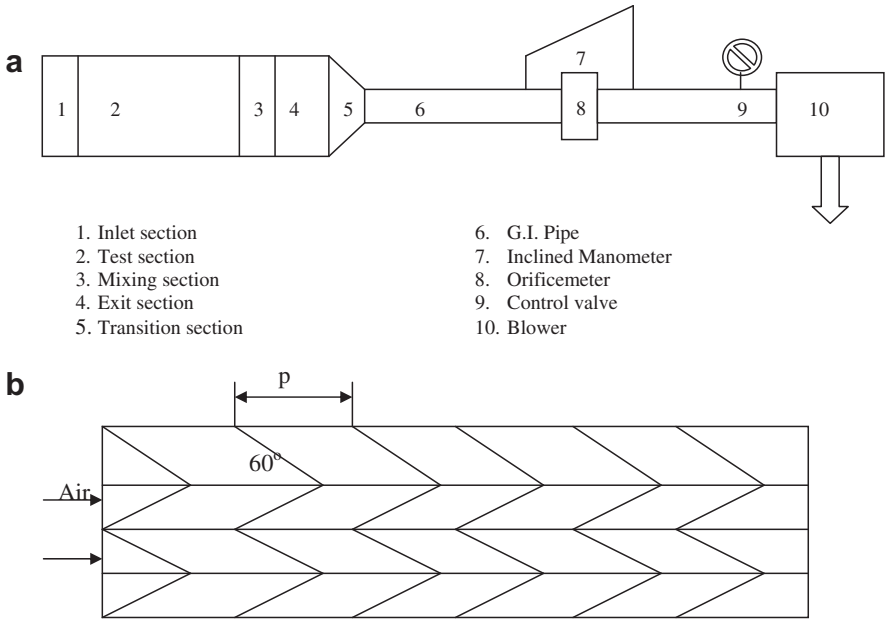

Fig. 1. (a) Schematic diagram of experimental set up. (b) Schematic diagram of 60° W-shaped ribs.

Range of Reynolds number and relative roughness height (e/D_h) has been chosen based on requirement of solar air heater [2].

Sixteen roughened plates as detailed in Table 1 have been tested; each set consisting of 07 runs with different flow rates covering Reynolds number range 2300–14,000. Validity test has been conducted on conventional smooth absorber plate under similar overall duct geometrical and flow conditions to serve as basis of comparison of results with values for heat transfer and friction factor from correlations available for smooth duct in literature. Air is sucked through rectangular duct by means of blower and gate valve has been used to control amount of air in duct. Air is thoroughly mixed in mixing chamber and baffles have been provided for achieving thorough mixing of air. Outside of entire set up from test section inlet to orifice plate has been insulated with thermocole. Upper side of duct has been covered with black insulating material to minimize thermal losses to environment and thus it ensures that all energy supplied from heater is transferred to duct. Other end of duct has been connected to circular pipe via rectangular to circular transition section. Flow rate of air in duct has been measured by means of flange type orifice meter. Pressure drop across orifice meter has been measured by inclined U-tube manometer. Pressure drop in test section has been measured by micro-manometer. Two pressure taps located along axial centerline of smooth lower wall of test section have been used to measure pressure drop across 1.36 m length of test section. Calibrated Copper Constantan (28 ASWG) thermocouples have been used for measurement of average plate temperatures, average fluid temperatures in the duct, inlet and outlet air temperatures. Digital micro-voltmeter has been used for measurement of thermocouple output through selector switch. Fig. 2 shows position of thermocouples on absorbing plate.

Before starting the experiment, all instruments and components of experimental set up have been checked for proper operation. After switching on blower, joints of set up have been checked for air leakage. After assembling the roughened plate, energy for heating is supplied to roughened entrance section and to test section. Data have been noted under steady state condition which has been assumed to have reached when plate and air temperatures showed negligible variation for around 10 min duration. Steady state for each test run has been obtained in about 1.5–2 h.

Table 1
Values of parameters.

Sr. No	Parameters	Values
1	Relative roughness pitch (p/e)	10 (for each plate)
2	Rib height (e)	0.8 mm, 1.0 mm, 1.3 mm & 1.5 mm
3	Relative roughness height (e/D_h)	0.018, 0.0225, 0.02925 & 0.03375
4	Duct aspect ratio (W/H)	8
5	Reynolds number (Re)	2300–14,000 (for each plate)
6	Angle of attack (α)	30°, 45°, 60° & 75°

3. Data reduction

Steady state values of plate and air temperatures at various locations have been obtained for given heat flux and mass flow rate of air. Heat transfer rate to air, Nusselt number and friction factor have been computed from the data. These values have been used to investigate effect of various influencing parameters such as flow rate and angle of attack of flow on Nusselt number and friction factor.

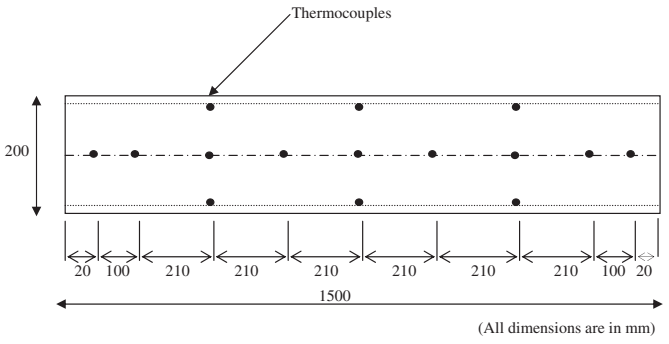

Fig. 2. Position of thermocouples on absorbing plate (test length).

Following equations have been used for the evaluation of relevant parameters

$$q = m \times C_p \times (t_o - t_i) \quad (1)$$

$$h = q/\left[A_c \times \left(t_p - t_f\right)\right] \quad (2)$$

$$Nu_r = (h \times D_h)/k \quad (3)$$

$$f_r = D_h \times \Delta p/\left(2 \times L \times V^2 \times \rho\right) \quad (4)$$

Uncertainty analysis as proposed by Kline and McClintock [38] has been used for prediction of uncertainty associated with experimental result. Following values give uncertainty in values of important parameters namely Reynolds number (Re), Nusselt number (Nu_r) and friction factor (f_r):

Parameter	Uncertainty (%)
Re	1.57%
Nu_r	5.77%
f_r	3.17%

4. Results and discussion

Fig. 3 shows variation of plate temperature and fluid temperature in duct. Temperature t_p and t_f are average values of absorber plate temperature and fluid temperature respectively. Average value of plate temperature (t_p) has been determined from temperature measured at nine locations on plate as shown in Fig. 2. Average fluid temperature t_f is average of inlet and outlet temperatures. Figs. 4 and 5 show comparison of experimental values and those predicted by correlations for Nusselt number and friction factor of smooth duct proposed by modified Dittus Boelter correlation for Nusselt number and by modified Blasius correlation for friction factor. In case of smooth duct for Reynolds number range applicable for solar air heater, Altfeld et al. [39] suggested that

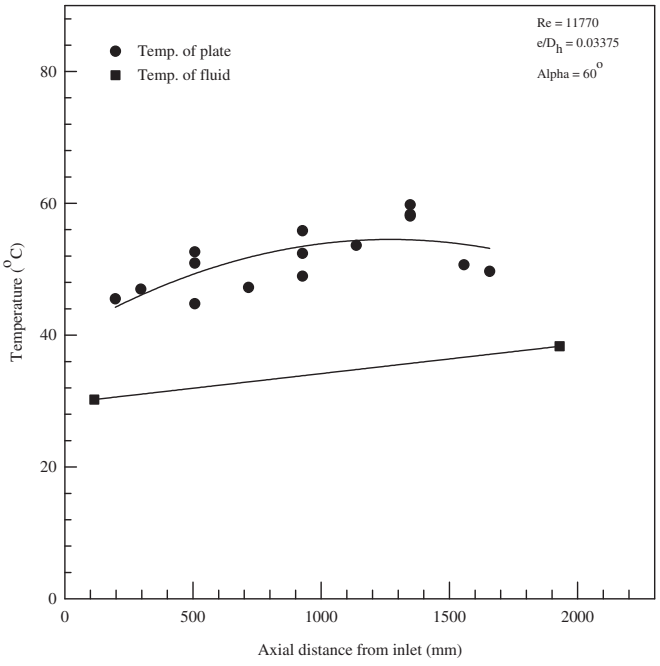

Fig. 3. Plate and air temperature distribution along length of test duct.

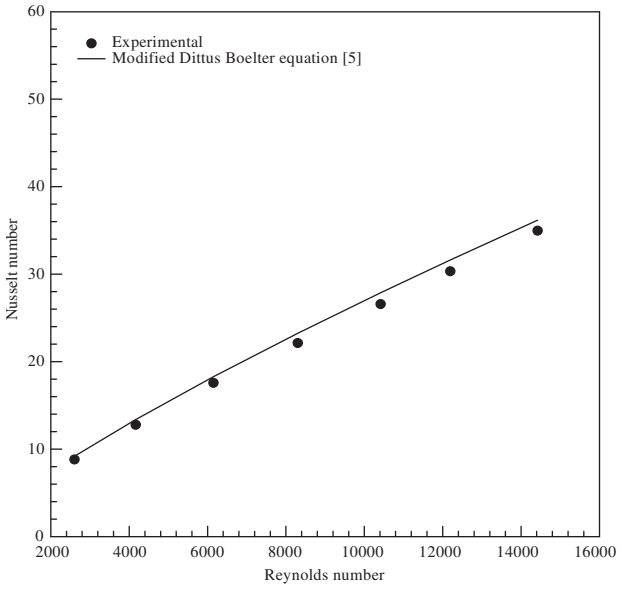

Fig. 4. Comparison of experimental values and predicted values of Nusselt number for smooth duct.

modified Blasius correlation for friction factor can be used. For Nusselt number of smooth duct [40].

$$Nu_s = 0.023 \times \mathrm{Re}^{0.8} \times \mathrm{Pr}^{0.4} \times (2R_{av}/D_e)^{-0.2} \quad (5)$$

where $2R_{av}/\mathrm{D_e} = (1.156 + \mathrm{H/W} - 1)/(\mathrm{H/W})$ for rectangular channel.

For friction factor

$$f_s = 0.085 \times (\mathrm{Re})^{-0.25} \quad (6)$$

Absolute percentage deviation between predicted and experimental results has been found to be ±5% for Nusselt number and friction factor. Excellent agreement between experimental and predicted values establishes accuracy of measurement on experimental test rig.

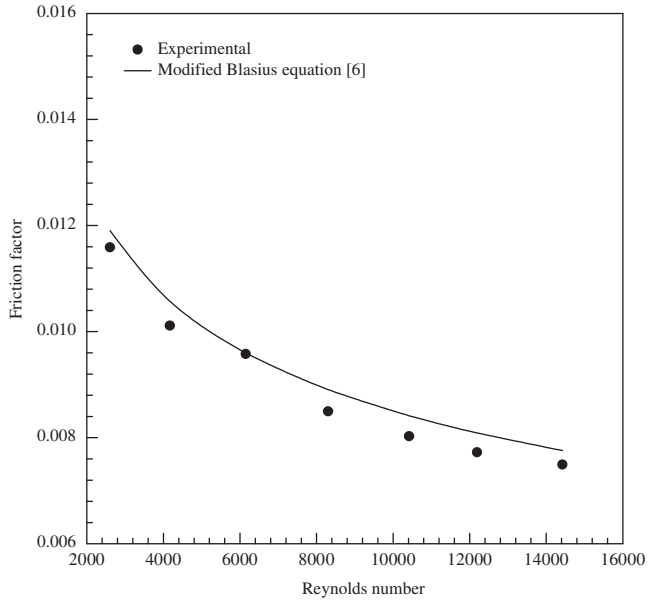

Fig. 5. Comparison of experimental values and predicted values of friction factor for smooth duct.

Variation of Nusselt number and friction factor with Reynolds number, relative roughness height and angle of attack of flow are shown in Figs. 6–11. Results are discussed below.

4.1. Effect of Reynolds number

Figs. 6 and 7 show effect of Reynolds number on Nusselt number and friction factor respectively. Nusselt number increases whereas friction factor decreases with an increase of Reynolds number as expected. But values of Nusselt number and friction factor are different as compared to those for smooth plate due to change in fluid flow characteristics as result of roughness which causes flow separation, reattachment and generation of secondary flows.

In early studies carried out by Nikuradse [41] and outlined in thesis of Gupta [42] and as well stated by Momin et al. [27] following are flow regimes with respect to artificially roughened surfaces:

Range I: Hydraulically smooth flow regime
$(0 \leq e^{+} \leq 5)$;

Range II: Transitionally rough flow regime
$(5 \leq e^{+} \leq 70)$;

Range III: Completely rough flow regime
$(e^{+} > 70)$.

In hydraulically smooth flow regime i.e., for low Reynolds number roughness has no effect on friction factor for all values of relative roughness height. Projections of roughness elements lie entirely within laminar sub-layer. In transition rough flow regime, influence of roughness becomes noticeable to an increasing degree. It is particularly characterized by the fact that friction factor depends upon Reynolds number as well as upon relative roughness height. Thickness of laminar sub-layer is of same order of magnitude as height of roughness elements in transition rough flow regime. In completely rough flow regime, friction factor becomes independent of Reynolds number and curve for friction factor vs Reynolds number becomes parallel to horizontal axis. All projections of roughness elements extend beyond laminar sub-layer as thickness of boundary layer becomes small in comparison to roughness height. In present investigation flow lies in transitionally rough flow regime. Flow is therefore characterized by flow Reynolds number resulting in laminar boundary layer of thickness of same order of magnitude as roughness height. This is usually done to keep friction losses in check although highest Nusselt number values cannot be expected. However as seen from Fig. 6, enhancements are noticeable and justify use of artificial roughness. Maximum enhancement of Nusselt number has been found to be 1.76, 2.01, 2.02 and 1.93 times that for smooth duct for angles of attack of 30°, 45°, 60° and 75° respectively for relative roughness height of

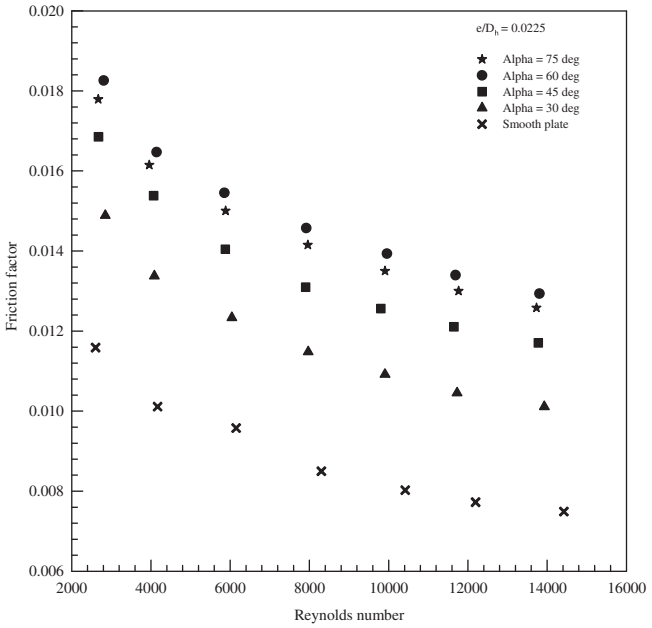

Fig. 7. Effect of Reynolds number on friction factor for relative roughness height of 0.0225 and for given angle of attack of flow.

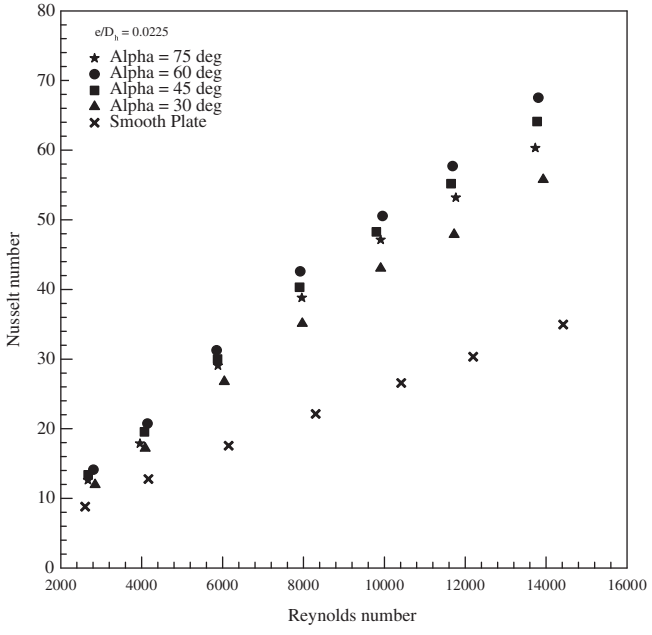

Fig. 6. Effect of Reynolds number on Nusselt number for relative roughness height of 0.0225 and for given angle of attack of flow.

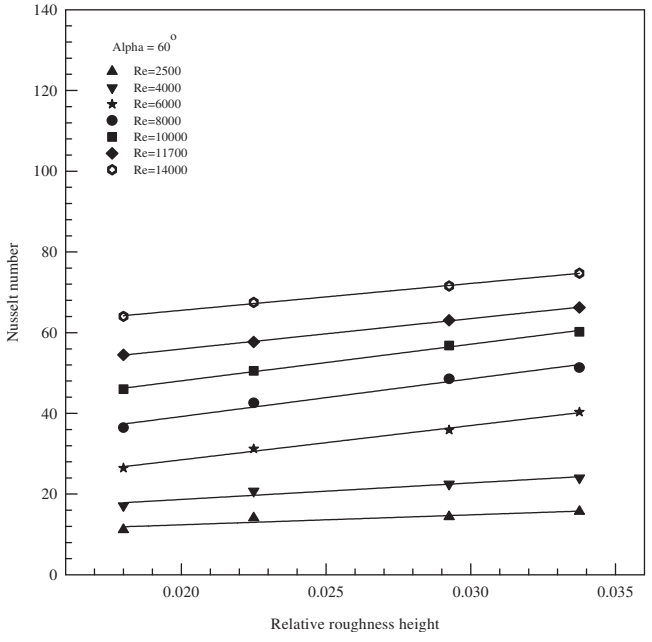

Fig. 8. Effect of relative roughness height on Nusselt number for given Reynolds number and for angle of attack of flow of 60°.

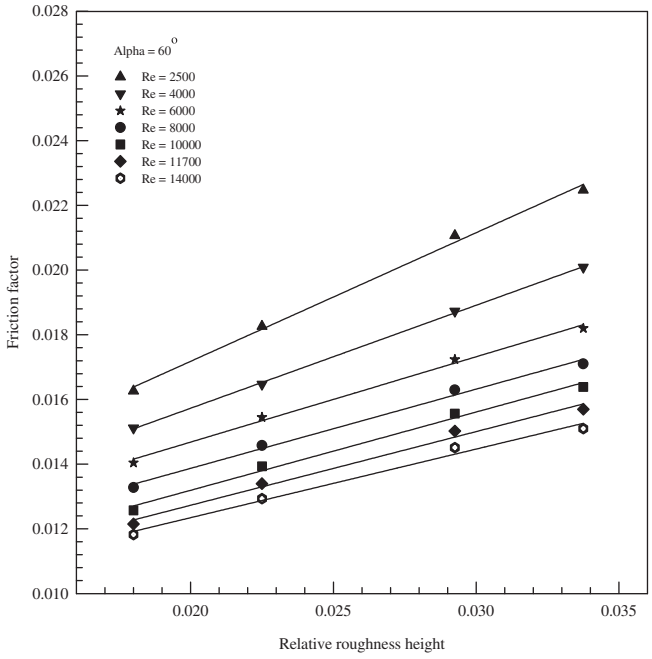

Fig. 9. Effect of relative roughness height on friction factor for given Reynolds number and for angle of attack of flow of 60°.

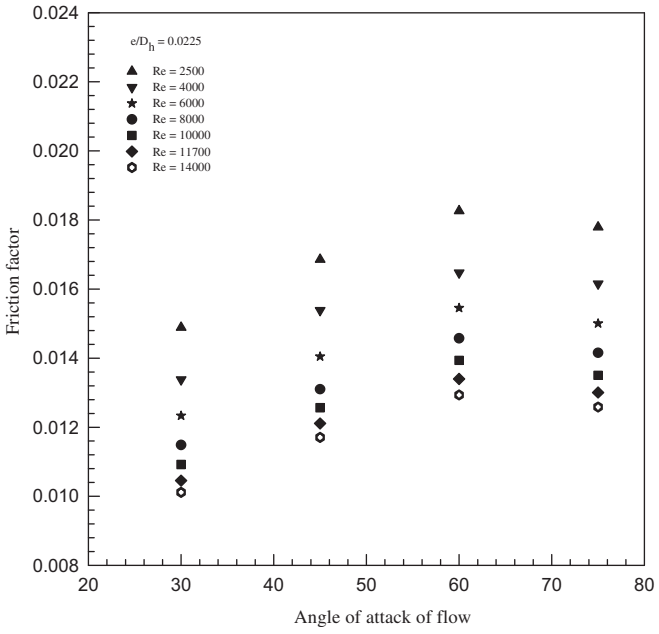

Fig. 11. Effect of angle of attack of flow on friction factor for relative roughness height of 0.0225 and for given Reynolds number.

0.0225. For relative roughness height of 0.03375, maximum enhancement of Nusselt number has been found to be 1.99, 2.28, 2.36 and 2.23 times that for smooth duct for angles of attack of 30°, 45°, 60° and 75° respectively. Maximum enhancement in friction factor has been found to be 1.36, 1.57, 1.72 and 1.68 times that for smooth duct for angles of attack of 30°, 45°, 60° and 75° respectively for relative roughness height of 0.0225. For relative roughness height of 0.03375, maximum enhancement in friction factor has been found to be 1.67, 1.86, 2.01 and 2.00 times that for smooth duct for angles of attack of 30°, 45°, 60° and 75° respectively.

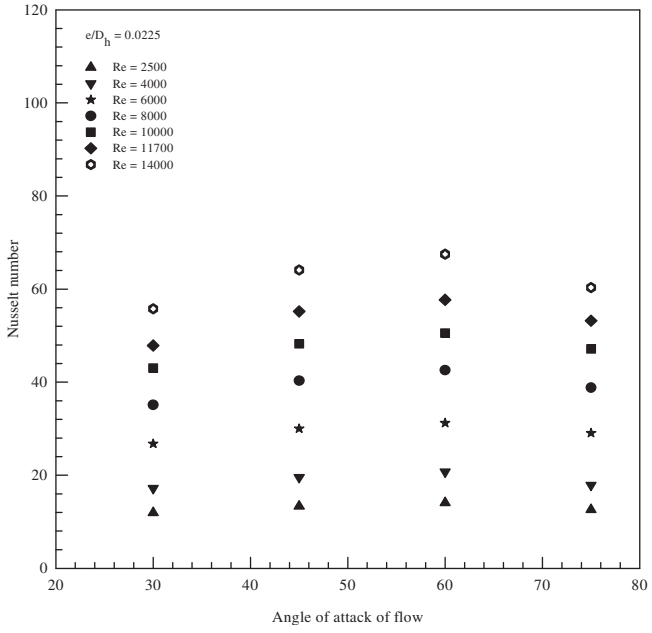

Fig. 10. Effect of angle of attack of flow on Nusselt number for relative roughness height of 0.0225 and for given Reynolds number.

4.2. Effect of relative roughness height

Effect of relative roughness height on Nusselt number and friction factor is shown in Figs. 8 and 9 respectively. It is seen that increase in relative roughness height results in increase in heat transfer coefficient and friction factor. Further it is seen that rate of increase of Nusselt number is lower than that of friction factor. This may be due to the fact that at higher values of relative roughness height, reattachment of free shear layer might not occur and rate of heat transfer enhancement is not proportional to that of friction factor as stated by Gupta et al. [22], Saini and Saini [23] and Momin et al. [27].

4.3. Effect of angle of attack of flow

Nusselt number and friction factor as function of angle of attack of flow are shown in Figs. 10 and 11 respectively. Maximum enhancement of Nusselt number and friction factor as result of providing artificial roughness has been found to be respectively 2.36 and 2.01 times that of smooth duct for angle of attack of 60°. It is observed that there exists an angle of attack that corresponds to maximum value of both Nusselt number and friction factor. Flow separation in secondary flow as result of W-shaped ribs and movement of resulting vortices combine to yield an optimum value of angle of attack. Results are in broad agreement with previous investigations both on angled straight ribs [22] and V-shaped ribs [27].

5. Thermo-hydraulic performance

Artificial roughness on absorber plate results in enhancement of heat transfer. Enhancement is accompanied by increase in friction factor. Hence roughness geometry has to be so selected such that heat transfer is maximized while friction losses are at minimum value. This is fulfilled by considering heat transfer and friction characteristics simultaneously. Parameter that facilitates simultaneous consideration of thermal and hydraulic performance is given

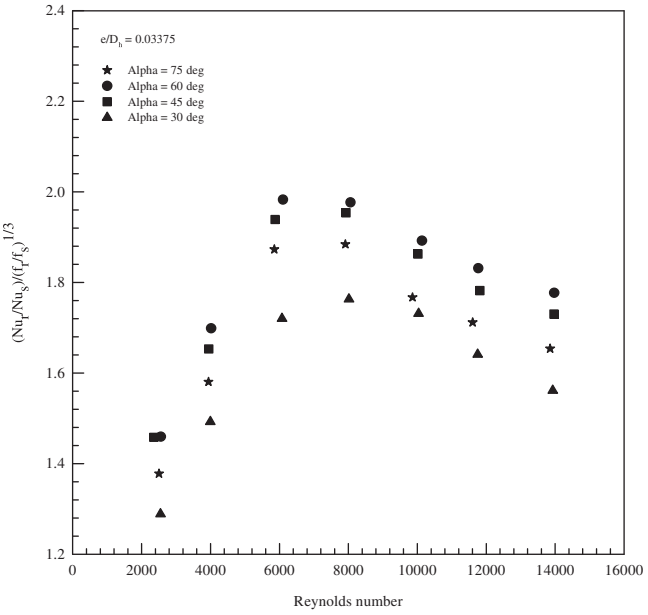

Fig. 12. Effect of Reynolds number on thermo-hydraulic performance parameter for relative roughness height of 0.03375 and for given angle of attack of flow.

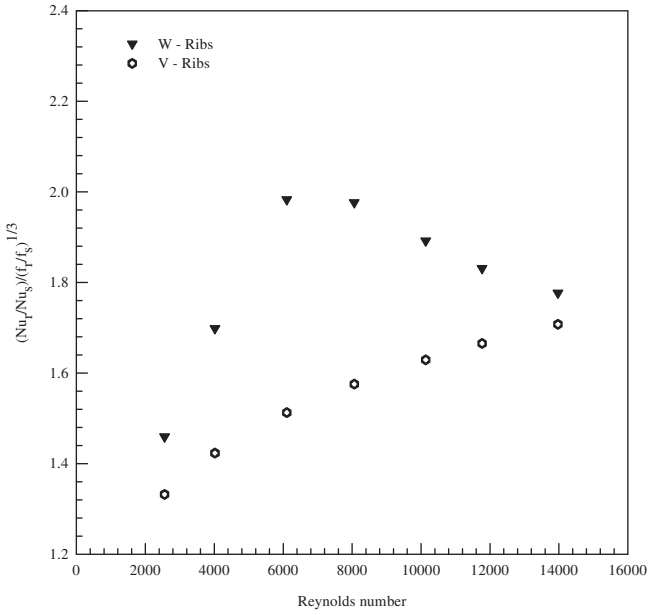

Fig. 14. Effect of Reynolds number on thermo-hydraulic performance parameter for W-shaped and V-shaped ribs for angle of attack of 60° and relative roughness height of 0.03375.

by Webb and Eckert [43] as $(Nu_r/Nu_s)/(f_r/f_s)^{1/3}$. This parameter is plotted in Fig. 12 against Reynolds number for relative roughness height of 0.03375 and for different angles of attack. It is seen that in general thermo-hydraulic performance improves with increasing angle of attack and absolute maxima occurs for angle of attack of 60°. But for given value of angle of attack there is a maxima corresponding to certain value of Reynolds number. Also as relative roughness height is increased thermo-hydraulic parameter increases in range of values investigated as shown in Fig. 13.

Fig. 14 has been drawn to show increase in thermo-hydraulic performance achieved by using W-shaped roughness geometry. Comparison of experimental values of thermo-hydraulic performance parameter as function of Reynolds number has been drawn for W-shaped 60° ribs and for V-shaped 60° ribs [27]. Data used for V-shaped ribs has been generated from correlation available in literature [27]. It is seen that thermo-hydraulic performance of W-ribs is superior to V-ribs. Ribs in W-configuration are shorter than ribs of V-shaped configuration for same width of plate so boundary layer along relatively shorter W-ribs is thinner than boundary layer along V-shape ribs. Hence enhancement is more in W-shaped ribs than in V-shaped ribs.

6. Correlations for Nusselt number and friction factor

From Figs. 6–11, it is seen that Nusselt number and friction factor are a strong functions of system and operating parameters of roughened duct, namely Reynolds number (Re), relative roughness

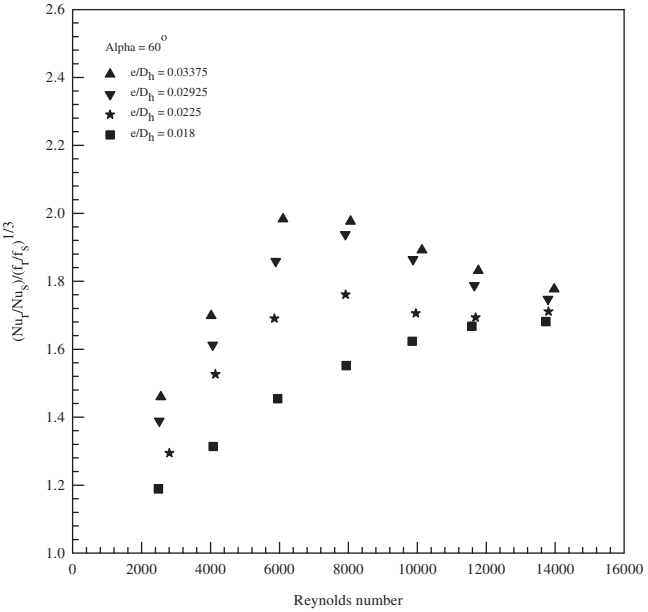

Fig. 13. Effect of Reynolds number on thermo-hydraulic performance parameter for angle of attack of 60° and for given relative roughness height.

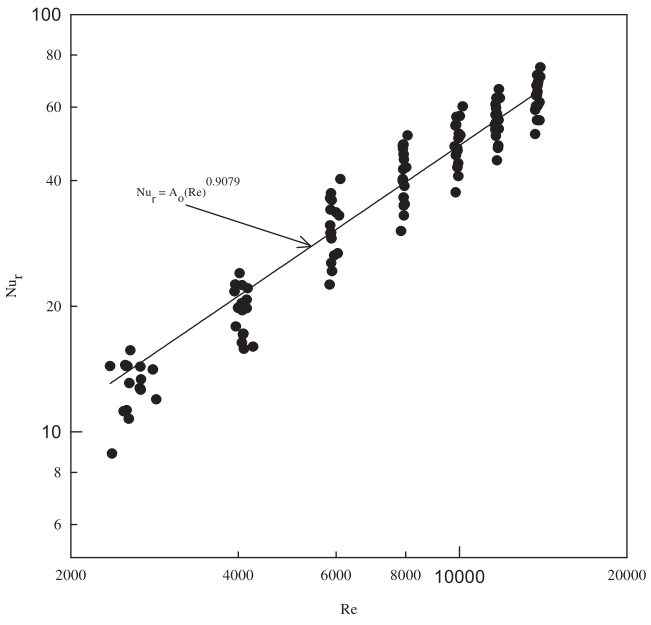

Fig. 15. Nusselt number vs. Reynolds number for 112 data points.

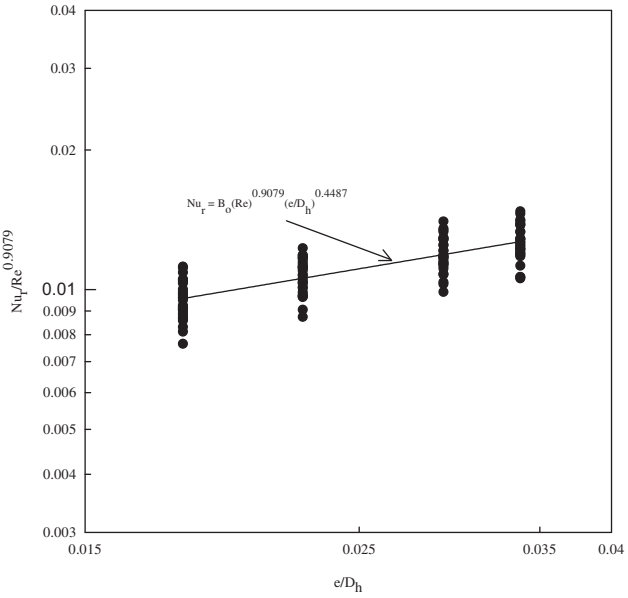

Fig. 16. Plot of $Nu_r/\mathrm{Re}^{0.9079}$ vs. e/D_h.

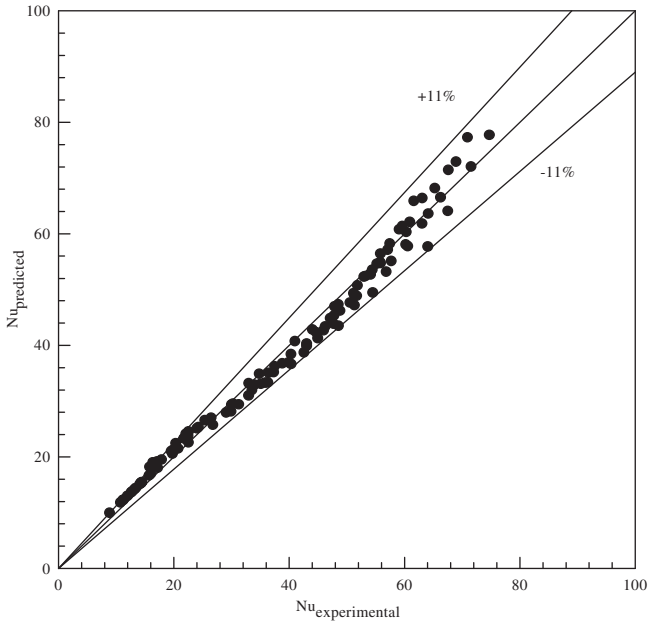

Fig. 18. Nusselt number (predicted) vs. Nusselt number (experimental).

height (e/D_h) and angle of attack of flow (α). Functional relationships for Nusselt number and friction factor can be written as

$$Nu_r = f(\mathrm{Re}, e/D_h, \alpha) \tag{7}$$

$$f_r = f(\mathrm{Re}, e/D_h, \alpha) \tag{8}$$

Correlations have been developed as a function of system and operating parameters on similar lines of Saini and Saini [23] and Hsieh et al. [44]. Data corresponding to all 16 roughened plates totaling 112 data points have been used for regression analysis to fit second order polynomial. Fig. 15 shows Nusselt number as function of Reynolds number. Regression analysis to fit straight line through these data points gives

$$Nu_r = A_o(\mathrm{Re})^{0.9079} \tag{9}$$

Constant (A_o) is a function of other parameters i.e. relative roughness height (e/D_h). $\mathrm{Nu_r}/Re^{0.9079}$ ($=A_o$) is plotted in Fig. 16 as a function of relative roughness height (e/D_h) and by regression analysis it has been obtained as

$$\frac{Nu_r}{(\mathrm{Re})^{0.9079}} = B_o(e/D_h)^{0.4487} \tag{10}$$

Constant (B_o) is a function of angle of attack (α), so values of $\mathrm{Nu_r}/[(Re)^{0.9079} \times (e/D_h)^{0.4487}]$ are plotted in Fig. 17 as a function of ($\alpha/60°$). On regression analysis to fit second order polynomial, it has been obtained as

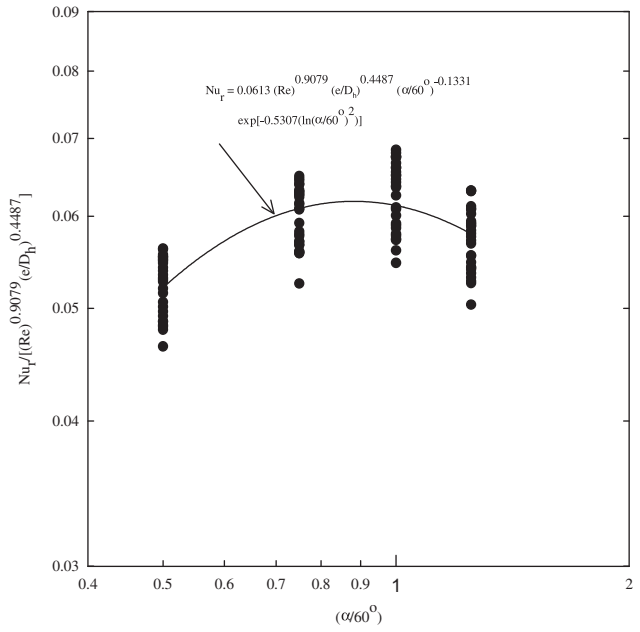

Fig. 17. Plot of $Nu_r/[\mathrm{Re}^{0.9079} \times (e/D_h)^{0.4487}]$ vs. ($\alpha/60°$).

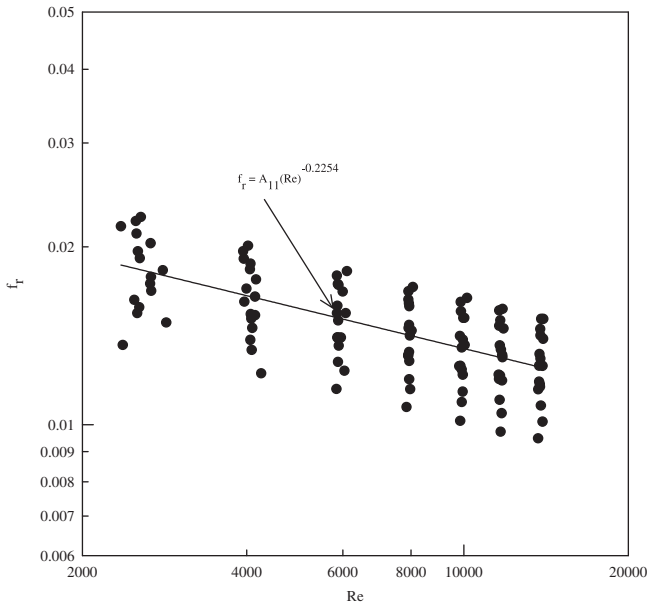

Fig. 19. Friction factor vs. Reynolds number for 112 data points.

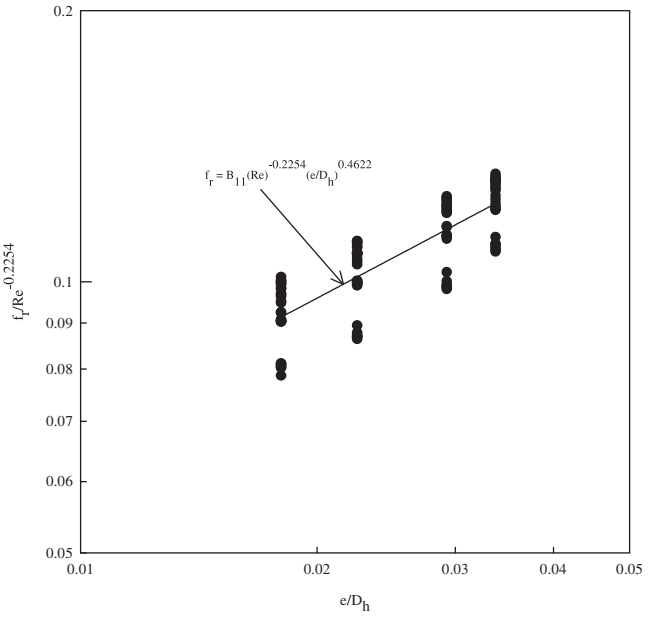

Fig. 20. Plot of $f_r/\mathrm{Re}^{-0.2254}$ vs. e/D_h.

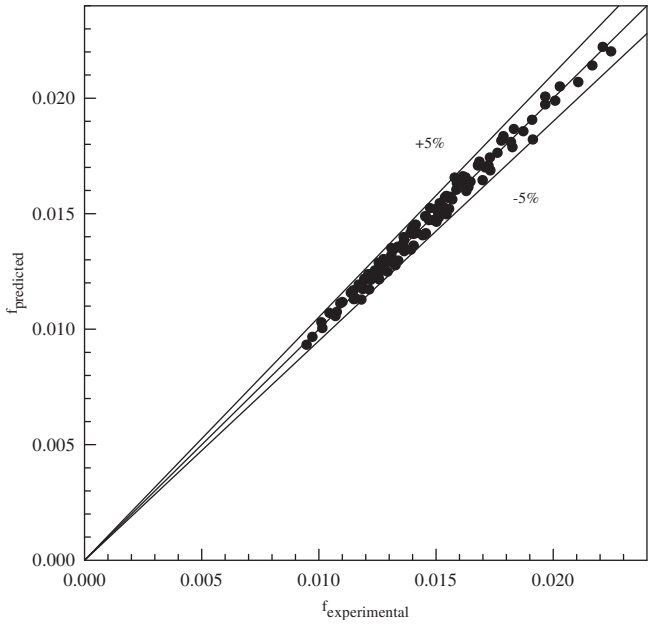

Fig. 22. Friction factor (predicted) vs. friction factor (experimental).

$$\log\left(\frac{Nu_r}{(\mathrm{Re})^{0.9079}(e/D_h)^{0.4487}}\right) = \log C_o + C_1\left(\log\left(\frac{\alpha}{60}\right)\right) + C_2\left(\log\left(\frac{\alpha}{60}\right)\right)^2 \quad (11)$$

where C_o, C_1 and C_2 are constants obtained from regression analysis. Finally converting Eq. (11) into appropriate form one can write as

$$Nu_r = 0.0613(\mathrm{Re})^{0.9079}(e/D_h)^{0.4487}\left(\frac{\alpha}{60}\right)^{-0.1331} \times \left[\exp\left(-0.5307\left(\ln\left(\frac{\alpha}{60}\right)\right)^2\right)\right] \quad (12)$$

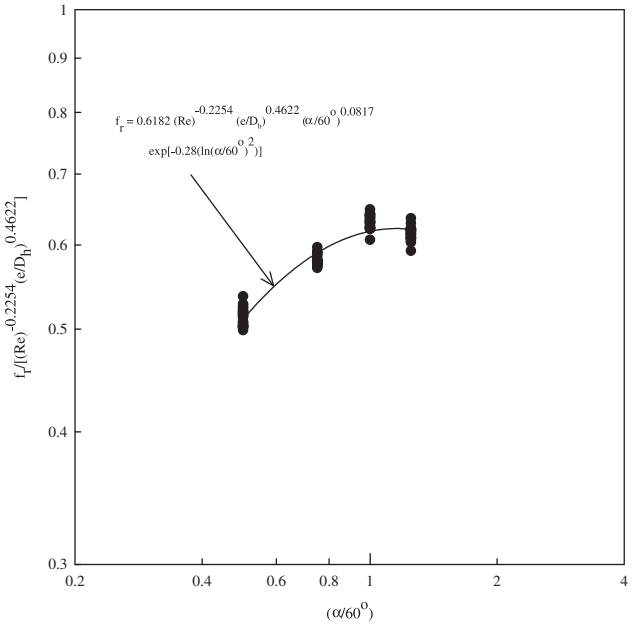

Fig. 21. Plot of $f_r/[\mathrm{Re}^{-0.2254} \times e/D_h{}^{0.4622}]$ vs. $\alpha/60°$).

Regression data relevant to this correlation is

(a) Average absolute percentage deviation: 5.23
(b) Regression coefficient: 0.92

Fig. 18 shows plot of experimental values and values predicted using Eq. (12). It can be seen that 106 data points out of 112 points lie within deviation line ±11%.

Similar procedure has been employed and correlation for friction factor has been developed. Figs. 19–21 have been used to develop correlation in following form:

$$f_r = 0.6182(\mathrm{Re})^{-0.2254}(e/D_h)^{0.4622}\left(\frac{\alpha}{60}\right)^{0.0817} \times \left[\exp\left(-0.28\left(\ln\left(\frac{\alpha}{60}\right)\right)^2\right)\right] \quad (13)$$

Regression data relevant to this correlation is:

(a) Average absolute percentage deviation: 0.01
(b) Regression coefficient: 0.93

Fig. 22 shows plot of experimental values and values predicted using Eq. (13) for friction factor.

It can be seen that 112 data points out of 112 points for friction factor lie within deviation lines of ±5%. Hence correlations developed are satisfactory for prediction of Nusselt number and friction factor of roughened duct with fairly good accuracy in range of parameters investigated.

7. Conclusions

1. Nusselt number increases whereas friction factor decreases with increase of Reynolds number. Values of friction factor and Nusselt number are higher as compared to those for smooth absorber plate. This is due to change in flow characteristics because of roughness that causes flow separation, reattachments and generation of secondary flow.

2. Rate of increase of Nusselt number with increasing Reynolds number is lower than rate of increase of friction factor because at higher values of relative roughness height, reattachment of free shear layer does not occur and rate of heat transfer enhancement is not proportional to that of friction factor.
3. Maximum enhancement of Nusselt number and friction factor as result of providing artificial roughness has been found to be respectively 2.36 and 2.01 times that of smooth duct for angle of attack of 60°. Same angle of attack corresponds to maximum values of both Nusselt number and friction factor. Flow separation and secondary flow resulting from presence of W-shaped ribs and movement of vortices combine to give optimum value of angle of attack.
4. Thermo-hydraulic performance improves with angle of attack of flow and relative roughness height and maxima occurs at angle of attack of 60°.
5. For relative roughness height of 0.03375 and at angle of attack of 60°, W-shape ribs enhance value of Nusselt number by 2.21 times over smooth plate at Reynolds number of 14,000.
6. Comparison of experimental values of Nusselt number and those predicted by correlation show that 106 out of 112 data points lie within deviation range of ±11% whereas in case of friction factor, 112 out of 112 data points lie within ±5%. It can therefore be concluded that correlations for prediction of Nusselt number and friction factor are reasonably satisfactory.

Nomenclature

A_c	surface area of absorber plate (m^2)
C_p	specific heat of air at constant pressure (J/kg K)
D_h	hydraulic diameter of air passage = 4WH/2(W + H) (m)
e	rib height (m)
e^+	roughness Reynolds number
f_r	average friction factor of roughened duct
f_s	average friction factor of smooth duct
h	convective heat transfer coefficient (W/m^2 K)
H	height of air duct (m)
k	thermal conductivity of air (W/m K)
L	test length (m)
m	mass flow rate of air (kg/s)
Nu_r	Average Nusselt number of roughened duct
Nu_s	Average Nusselt number of smooth duct
p	rib pitch (m)
Pr	Prandtl number
q	rate of heat transfer to air (W)
Re	Reynolds number
t_f	average temperature of fluid (°C)
t_p	average temperature of absorbing plate (°C)
t_i	average inlet temperature of air (°C)
t_o	average outlet temperature of air (°C)
V	velocity of air in the duct (m/s)
W	width of air duct (m)

Greek symbols

Δp	pressure drop in test length (Pa)
α	rib angle of attack (o)
ρ	density of air (kg/m^3)

Subscripts

r	rough
s	smooth

References

[1] Bhatti MS, Shah RK. Turbulent and transition flow convective heat transfer. In: Kakac S, Shah RK, Aung W, editors. Handbook of single phase convective heat transfer, Chapter 4. New York: John Wiley and Sons Inc; 1987.
[2] Saini JS. Use of artificial roughness for enhancing performance of solar air heater. In: Proceedings of XVII National and VI ISHME/ASME heat and mass transfer conference. Kalpakkam (India); January 05–07 2004. Kalpakkam (India). p. 103–12.
[3] Han JC. Heat transfer and friction in channels with two opposite rib roughened walls. J Heat Transfer 1984;106(4):774–81.
[4] Han JC. Heat transfer and friction characteristics in rectangular channels with rib turbulators. J Heat Transfer 1988;110(2):321–8.
[5] Han JC, Glicksman LR, Rohsenow WM. An investigation of heat transfer and friction for rib roughened surfaces. Int J Heat Mass Transfer 1978;21(8):1143–56.
[6] Han JC, Park JS, Lei CK. Heat transfer enhancement in channels with turbulence promoters. J Eng Gas Turbines Power 1985;107(3):628–35.
[7] Han JC, Zhang YM, Lee CP. Augmented heat transfer in square channels with parallel, crossed, and V-shaped angled ribs. J Heat Transfer 1991;113(3):590–6.
[8] Wright LM, Fu WL, Han JC. Thermal performance of angled, V-shaped, and W-shaped rib turbulators in rotating rectangular cooling channels (AR=4:1). J Turbomachinery 2004;126(4):604–14.
[9] Lau SC, Kukreja RT, Mcmillin RD. Effects of V-shaped rib arrays on turbulent heat transfer and friction of fully developed flow in a square channel. Int J Heat Mass Transfer 1991;34(7):1605–16.
[10] Lau SC, Mcmillin RD, Han JC. Turbulent heat transfer and friction in a square channel with discrete rib turbulators. J Turbomachinery 1991;113(3):360–6.
[11] Lau SC, Mcmillin RD, Han JC. Heat transfer characteristics of turbulent flow in a square channel with angled discrete ribs. J Turbomachinery 1991;113(3):367–74.
[12] Taslim ME, Bondi LA, Kercher DM. An experimental investigation of heat transfer in an orthogonally rotating channel roughened with 45 deg criss-cross ribs on two opposite walls. J Turbomachinery 1991;113(3):346–53.
[13] Taslim ME, Li T, Kercher DM. Experimental heat transfer and friction in channels roughened with angled, V-shaped, and discrete ribs on two opposite walls. J Turbomachinery 1996;118(1):20–8.
[14] Liou TM, Hwang JM. Effect of ridge shapes on turbulent heat transfer and friction in a rectangular channel. Int J Heat Mass Transfer 1993;36(4):931–40.
[15] Han JC, Park JS. Developing heat transfer in rectangular channels with rib turbulators. Int J Heat Mass Transfer 1988;31(1):183–95.
[16] Park JS, Han JC, Huang Y, Ou S, Boyle RJ. Heat transfer performance comparisons of five different rectangular channels with parallel angled ribs. Int J Heat Mass Transfer 1992;35(11):2891–903.
[17] Han JC, Zhang YM. High performance heat transfer ducts with parallel broken and V-shaped broken ribs. Int J Heat Mass Transfer 1992;35(2):513–23.
[18] Kiml R, Mochizuki S, Murata A. Effects of rib arrangements on heat transfer and flow behavior in a rectangular rib roughened passage: application to cooling of gas turbine blade trailing edge. J Heat Transfer 2001;123(4):675–81.
[19] Gao X, Sunden B. Heat transfer and pressure drop measurements in rib roughened rectangular ducts. Exp Thermal Fluid Sci 2001;24(1–2):25–34.
[20] Prasad K, Mullick SC. Heat transfer characteristics of a solar air heater used for drying purposes. Appl Energy 1983;13(2):83–93.
[21] Prasad BN, Saini JS. Effect of artificial roughness on heat transfer and friction factor in a solar air heater. Solar Energy 1988;41(6):555–60.
[22] Gupta D, Solanki SC, Saini JS. Heat and fluid flow in rectangular solar air heater ducts having transverse rib roughness on absorber plates. Solar Energy 1993;51(1):31–7.
[23] Saini RP, Saini JS. Heat transfer and friction factor correlations for artificially roughened ducts with expanded metal mesh as roughness element. Int J Heat Mass Transfer 1997;40(4):973–86.
[24] Karwa R, Solanki SC, Saini JS. Heat transfer coefficient and friction factor correlations for the transitional flow regime in rib-roughened rectangular ducts. Int J Heat Mass Transfer 1999;42(9):1597–615.
[25] Verma SK, Prasad BN. Investigation for the optimal thermo-hydraulic performance of artificially roughened solar air heaters. Renewable Energy 2000;20(1):19–36.
[26] Bhagoria JL, Saini JS, Solanki SC. Heat transfer coefficient and friction factor correlations for rectangular solar air heater duct having transverse wedge shaped rib roughness on the absorber plate. Renewable Energy 2002;25(3):341–69.
[27] Momin AME, Saini JS, Solanki SC. Heat transfer and friction in solar air heater duct with V-shaped rib roughness on absorber plate. Int J Heat Mass Transfer 2002;45(16):3383–96.
[28] Karwa R. Experimental studies of augmented heat transfer and friction in asymmetrically heated rectangular ducts with ribs on the heated wall in transverse, inclined, V-continuous and V-discrete pattern. Int Comm Heat Mass Tran 2003;30(2):241–50.
[29] Sahu MM, Bhagoria JL. Augmentation of heat transfer coefficient by using 90° broken transverse ribs on absorber plate of solar air heater. Renewable Energy 2005;30(13):2057–73.
[30] Jaurker AR, Saini JS, Gandhi BK. Heat transfer and friction characteristics of rectangular solar air heater duct using rig-grooved artificial roughness. Solar Energy 2006;80(8):895–907.

[31] Karmare SV, Tikekar AN. Heat transfer and friction factor correlation for artificially roughened duct with metal grit ribs. Int J Heat Mass Transfer 2007; 50(21–22):4342–51.
[32] Layek A, Saini JS, Solanki SC. Heat transfer and friction characteristics for artificially roughened ducts with compound turbulators. Int J Heat Mass Transfer 2007;50(23–24):4845–54.
[33] Aharwal KR, Gandhi BK, Saini JS. Experimental investigation on heat transfer enhancement due to a gap in an inclined continuous rib arrangement in a rectangular duct of solar air heater. Renewable Energy 2008;33(4):585–96.
[34] Varun, Saini RP, Singal SK. Investigation of thermal performance of solar air heater having roughness elements as a combination of inclined and transverse ribs on the absorber plate. Renewable Energy 2008;33(6):1398–405.
[35] Saini RP, Verma J. Heat transfer and friction factor correlations for a duct having dimple shape artificial roughness for solar air heaters. Energy 2008; 33(8):1277–87.
[36] Saini SK, Saini RP. Development of correlations for Nusselt number and friction factor for solar air heater with roughened duct having arc shaped wire as artificial roughness. Solar Energy 2008;82(12):1118–30.
[37] Duffie JA, Beckman WA. Solar energy thermal processes. New York: Wiley and Sons; 1980. p. 211.
[38] Kline SJ, McClintock FA. Describing uncertainties in single sample experiments. J Mech Eng 1953;75:3–8.
[39] Altfeld K, Leiner W, Fiebig M. Second law optimization of flat plate solar air heaters. Part 2: results of optimization and analysis of sensibility to variations of operating conditions. Solar Energy 1988;41(4):309–17.
[40] Kakac S, Shah RK, Aung W. Handbook of single phase convective heat transfer. New York: Wiley; 1987.
[41] Nikuradse J. Law of flow in rough pipes, vol. 1292. National Advisory Committee for Aeronautics Technical Memorandum; 1950.
[42] Gupta D. Investigations on fluid flow and heat transfer in solar air heaters with roughened absorbers. Ph.D. thesis: University of Roorkee. Roorkee (India); 1993.
[43] Webb RL, Eckert ERG, Goldstein RJ. Heat transfer and friction in tubes with repeated rib roughness. Int J Heat Mass Transfer 1971;14(4):601–17.
[44] Hsieh SS, Shih HJ, Hong YJ. Laminar forced convection from surface mounted ribs. Int J Heat Mass Transfer 1990;33(9):1987–99.